Grant Agreement No. 611373

FP7-ICT-2013-10

# D4.2. Implementation of cooperative control and formation keeping with diver in the loop

Due date of deliverable: 05/2016

Actual submission date: 05/2016

Start date of project: 01 January 2014 Duration: 36 months

Organization name of lead contractor for this deliverable: IST

Revision: version 1

| Dissemination level | | |
|---|---|---|
| PU | Public | x |
| PP | Restricted to other programme participants (including the Commission Services) | |
| RE | Restricted to a group specified by the consortium (including the Commission Services) | |
| CO | Confidential, only for members of the consortium (including the Commission Services) | |

# Contents

# 1 Outline of the deliverable

This deliverable describes the final control implementation of the buddy guide functionality that aims to guide human divers to a certain point or path. Such a behavior is done while waiting for the humans and being at all the time in the divers' field of view to maintain two-way communication.

Due to the vehicles' role nature, two completely very different control strategies were used, for underwater and surface vehicles and are reported in this document.

Simulations are here presented as well as results of sea trials, testing the system partially.

# 2 Surface vehicle control strategy – Artificial Potential Field

Bearing in mind the requirements that arise from the CADDY concept, there are two main scenarios that the surface vehicle should tackle in order to track the underwater segment:

- Buddy vehicle following diver: this scenario implies that both underwater agents are performing unstructured/random trajectories;
- Buddy vehicle surveying an area and diver at rest: in this scenario Buddy vehicle is performing a structured (lawnmower) trajectory while diver is stopped or has a random walk behavior.

According to these scenarios the underwater agents can perform any type of mission and therefore estimating its position can be an extremely difficult task and so, it is not possible for the surface vehicle to strictly follow the path taken by the other two agents as was done in (Abreu e Pascoal 2015) where the trajectories were generated online, but its types where predefined, thus making it possible to generate targets to track.

In CADDY instead, the surface vehicle is only expected to be in an area close-by in order to improve, among other things, the acoustic communications with the underwater agents, while avoiding being on top of them, for safety purposes. This strategy was already explained in (Nađ, et al. 2016).

To implement the above strategy in a way that both scenarios are contemplated, an artificial potential field (*APF*) technique was used. As can be seen in (Latombe 1991) and (Khatib 1985) an *APF* consists basically of the sum of potential fields, one attractive and one or more repulsive:

$$\boldsymbol{U} = \boldsymbol{U}_{att} + \boldsymbol{U}_{rep}^{B} + \boldsymbol{U}_{rep}^{D}$$

where $\boldsymbol{U}_{att}$ is the attractive potential and $\boldsymbol{U}_{rep}^{B}$ and $\boldsymbol{U}_{rep}^{D}$ are the repulsive potential generated by the BUDDY and the diver, respectively.

In this specific case, the idea was to create a potential field that has a basin sloped towards a circle around the midpoint between the BUDDY and the diver and a peak on top of each target with a flat area around it. With this configuration, instead of generating a global minimum point, a global minimum area is created which causes the surface vehicle to have a more relaxed behavior. The function that describes this potential field is given by:

$$\boldsymbol{U}_{att} = \begin{cases} 0, & \boldsymbol{p}_M \leq r_i \\ \left(\boldsymbol{p}_M - r_o + \frac{r_o - r_i}{2}\right)\lambda_a, & \boldsymbol{p}_M \geq r_i \\ \frac{\lambda_a}{2}\left[\boldsymbol{d} - sin\left(\frac{\boldsymbol{d}\pi}{r_o - r_i}\right)\frac{r_o - r_i}{\pi}\right], & \text{otherwise} \end{cases}$$

$$\boldsymbol{U}_{rep} = \begin{cases} 0, & \boldsymbol{p}_T \geq r_t \\ \left[cos\left(\frac{\boldsymbol{p}_T}{r_t}\frac{\pi}{2} + \frac{\pi}{2}\right) + 1\right]\frac{2\lambda_r r_t}{\pi}, & \text{otherwise} \end{cases}$$

where $\boldsymbol{p}_M$ is the vector between surface vehicle and the midpoint between the two underwater agents, $r_i$ is the radius of the flat area, $r_o$ is the radius where the basin reach its maximum derivative $\lambda_a$, $\boldsymbol{d}$ is the distance between the surface vehicle and $r_i$, $\boldsymbol{p}_T$ is the vector between the surface vehicle and one of the underwater agents, $r_t$ is the distance to the target where the peak starts to grow from zero and $\lambda_r$ is the maximum derivative of the repulsive potential.

An example of this *APF* is represented in Figure 2.1, where two virtual underwater agents are located at [-2.5; -2.5] and [2.5;2.5].

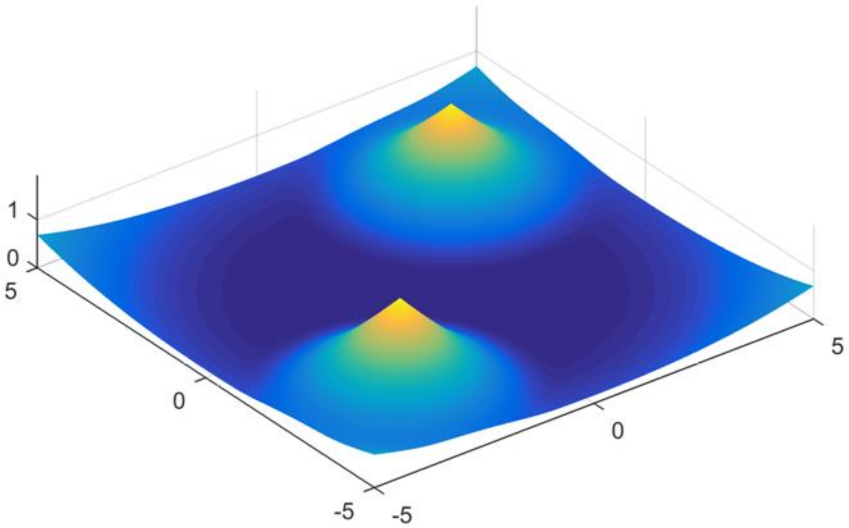


*a) 3D Representation of the APF*

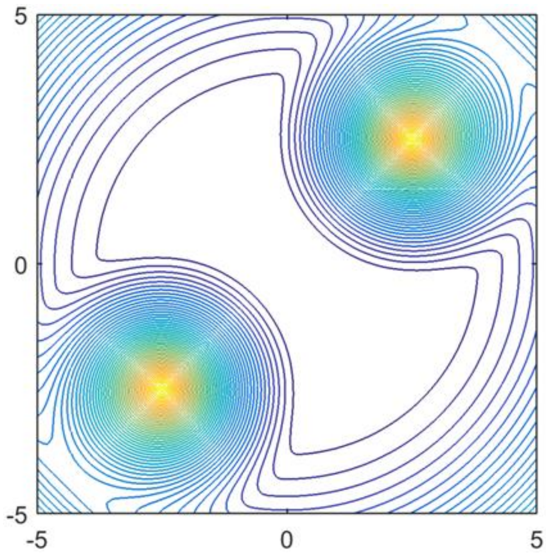


*b) Contour view of the APF*

*Figure 2.1 – Views of the APF when the two agents are far apart*

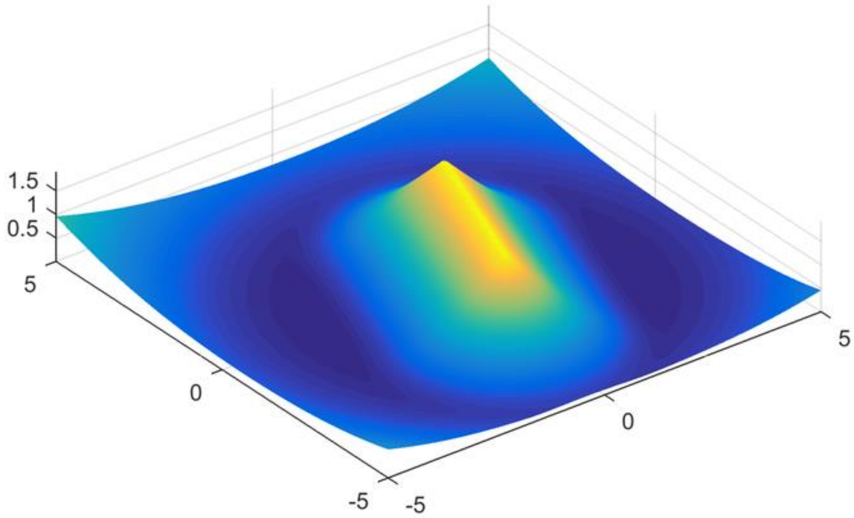


*a) 3D Representation of the APF*

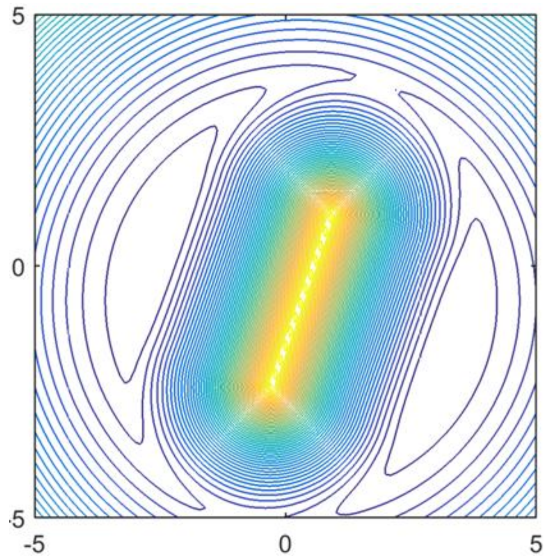


*b) Contour view of the APF*

*Figure 2.2 - Views of the APF panel*

However, with this approach, when the underwater agents are very close, the sum of the potential fields can generate some local minimum points and saddle points, which can cause problems in terms of convergence because it can attract and trap the surface vehicle. For this reason, when the underwater agents are close, instead of creating a potential field for each agent, a single potential connecting the two agents is generated. This type of potential function is known in fluid mechanics as *panel method* (Kuethe e Chow 1985) (Fahimi, Ashrafiuon e Nataraj 2003).

In Figure 2.2 an example of a *panel* is shown. In order to avoid a fast-switching between the two modes (*peaks* and *panel*) a hysteresis function, based on the distance between the two underwater agents, was implemented.

Finally, after the construction of the complete potential field it is possible to extract the desired velocity vector for the surface vehicle by calculating the negative gradient of the potential function.

# 3 Underwater vehicle control strategy – Pointer experiment

The pointer experiment, shown in Figure 3.1, requires the Buddy to position itself relative to the driver on a circular path. Movements must be executed on a safety circular path to avoid unplanned entry into diver's private space. The virtual target path following control method offers a simple controller structure for implementing this behaviour. The problem can be extended to incorporate positioning on the path in case of fully-actuated vehicles like Buddy.

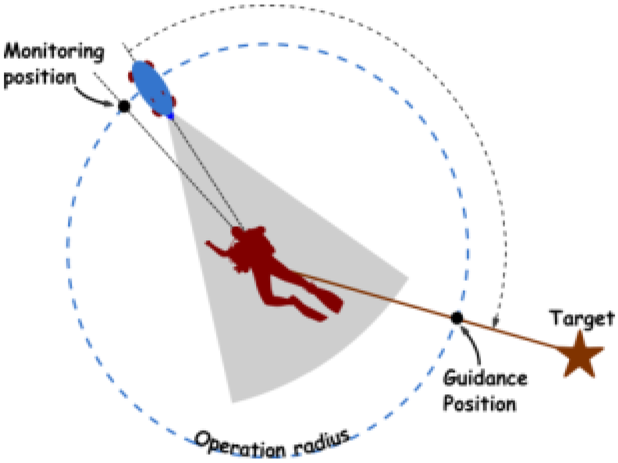


*Figure 3.1 - General pointer concept displaying the spatial distribution of Buddy, diver and the desired guidance target*

Deriving the controller requires defining three working frames. The navigation frame {N} is defined as the local tangent plane or North-East-Down frame and the vehicles and diver absolute position are defined in this frame. The body fixed frame, {B}, is connected the vehicle and moves within {N}. Finally, the path frame, {P}, axis are defined by a tangent unit vector $\vec{t}$ and the normal unit vector $\vec{n}$ at a path point $\varpi$. The main goal is to converge to the origin of {P}, thus ensuring the location on the safety path (circle) around the diver. The secondary goal is to have Buddy converge on a certain point of the path $\mu^*$ while continuing to face the diver.

The kinematic model of the distance to is described with

$$\dot{\mathbf{d}}^p = -\mathbf{S}_p^n \mathbf{d}^p + \mathbf{R}_\mathrm{b}^p \mathbf{v}^b - \mathbf{R}_n^p \dot{\mathbf{r}}^n - \dot{\tilde{\varpi}} \vec{\mathbf{t}} - \dot{\mu}^* \vec{\mathbf{t}}$$

where $\dot{\mathbf{d}}^p$ is the distance in {P}, $\mathbf{v}^b$ the Buddy speed in {B} and $\dot{\mathbf{r}}^n$ the diver speed in {N}. Lyapunov based design can be applied for deriving the kinematic controller. Consider the following control Laypunov function (CLF)

$$V = \frac{1}{2}\mathbf{d}^\mathrm{T}\mathbf{d} + \frac{\sigma}{\mathrm{k}} \ln \cosh \mathrm{k}\tilde{\varpi}$$

with tuneable gains σ and k larger than zero. The CLF gradient reduces to

$$\dot{V} = -\mathbf{d}^{\mathrm{T}}\mathbf{K_p}\mathbf{d} - \mathrm{k}_{\varpi}(\mathrm{s} - \sigma \tanh \mathrm{k}\tilde{\varpi})$$

which is negative semi-definite in the origin and can be shown to globally stabilize the system asymptotically. This controller derived in this manner stabilizes position of the vehicle, but the heading is controlled separately. However, the heading control is skipped since it represents a trivial control where the desired heading is always towards the diver.

Notice that the draw-back of the approach is that the diver position and orientation need to be known with good precision in order to assure a stable monitoring position. While the position can be acquired with some precision from the camera and sonar, the USBL position, due to noise, will not be enough to assure good tracking. The diver orientation and orientation rate of change will have to be estimated from the USBL data, sonar and video image processing.

# 4 Results

## 4.1 Artificial Potential Field

The data shown in this section is the result of sea trials during the second review meeting in Lisbon. Note that *APF* controller was used in a different scenario from the one described in this report, namely Buddy slave, where Buddy performs a mosaic. Moreover, only one agent was being tracked by the surface vehicle, as there was no diver in the water.

Figure 4.1 shows the potential field function used on these experiments. This figure represents a slice that was taken along an arbitrary direction, where the $x$ axis represents the distance, in meters, from the surface vehicle to the target to be tracked.

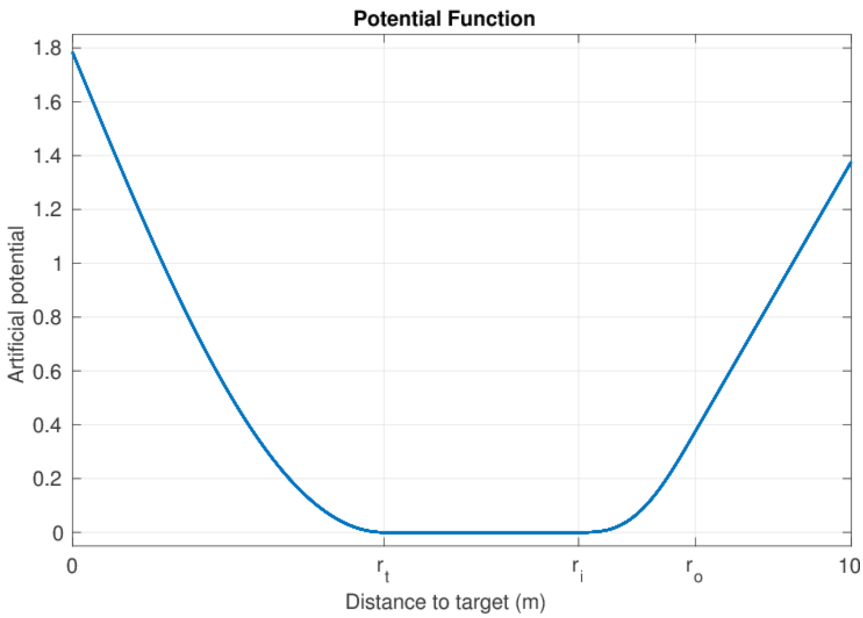


*Figure 4.1 - Slice of the potential function*

Figure 4.2 illustrates the velocity profile obtained by differentiating the potential function represented above. The parameters used to generate this potential function are: $r_o = 8\,m$, $\mathrm{r}_i = 6.5\,m$ , $\mathrm{r}_t = 4\,m$, $\lambda_a = 0.5\,m/s$ and $\lambda_r = 0.7\,m/s$.

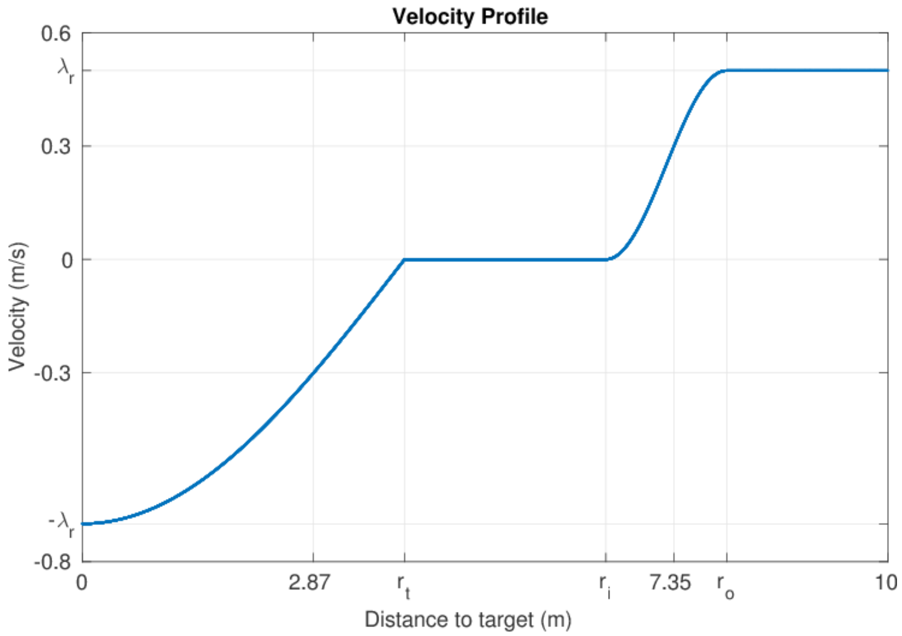


*Figure 4.2 - Velocity profile for the tracking controller*

As stated before, this velocity profile can be configured using some parameters, but in the end it is necessary to define the so-called *Equilibrium zone*. This zone is the expected operation region, where the surface vehicle is either stopped, giving support to the underwater agent, or moving at the same speed as the target. The limits of this area depend also on the maximum speed of the target being tracked, because when the whole system converges, the surface vehicle must have the same velocity as the underwater one. As can be seen in Figure 4.2 and knowing a priori that Buddy's maximum velocity is $0.3\,m/s$, the limits of the *Equilibrium zone* are $[2.87;\ 7.35]$.

To illustrate the application of this key concept, Figure 4.3 shows the inter-vehicle distance over time and the upper and lower limit of the *Equilibrium zone*.

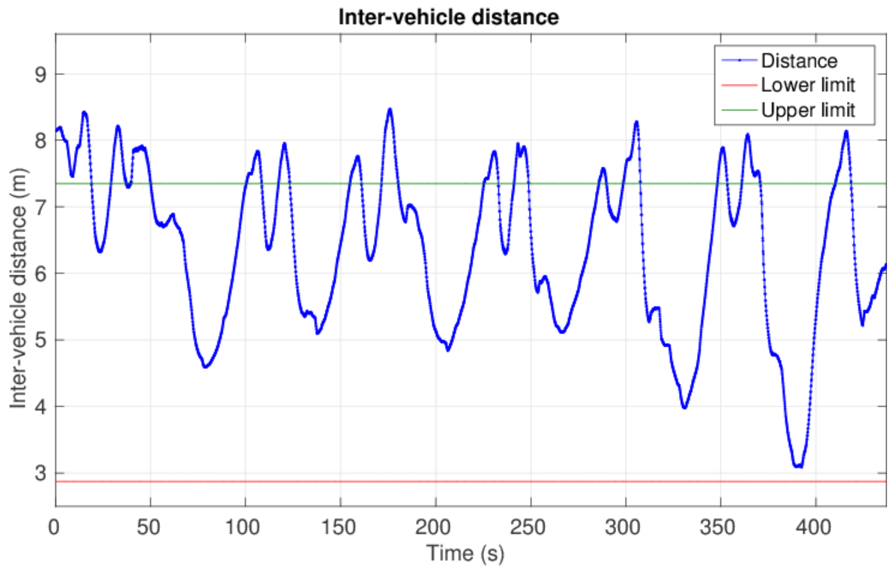


*Figure 4.3 - Tracking controller performance*

In order to have a better idea of the obtained error, in Figure 4.4 is shown the difference between the inter-vehicle distance and the *Equilibrium zone*.

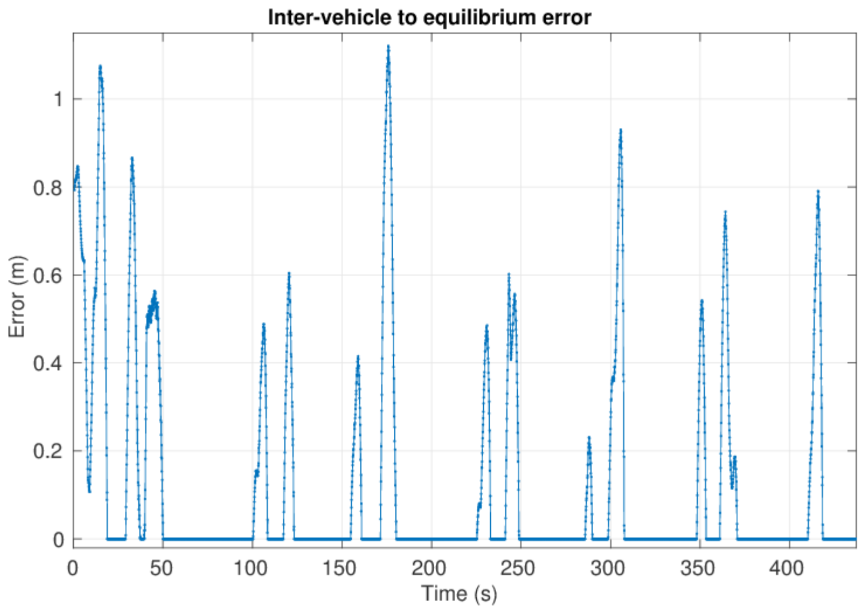


*Figure 4.4 - Error between inter-vehicle distance and the Equilibrium zone*

As can be seen, the overall performance was good with a maximum error of 1.1 meters. The controller can be tuned to improve the performance, but since the acoustic period is too high and the measured acoustic bearing is very erroneous, a set of very relaxed parameters were used to avoid aggressive control actions. Its trajectory can be assessed in Figure 4.5

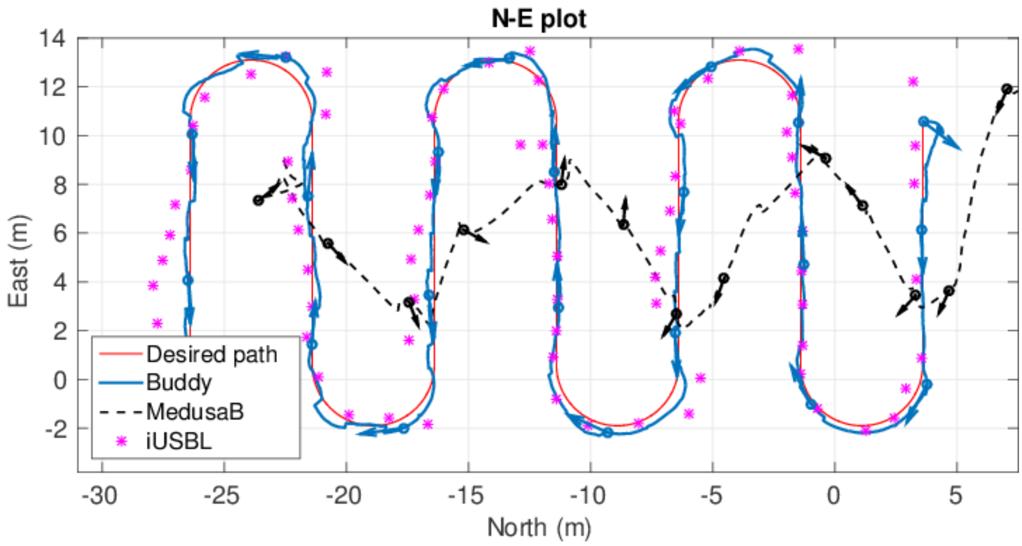


*Figure 4.5 - APF tracking controller performance*

## 4.2 Pointer Experiment

During trials in October 2015 the algorithm was tested using the virtual diver and USV simulated driver. The virtual diver approach included a simulated diver position and the Buddy AUV operated in real conditions. The method is a first step towards real implementation and is used to evaluate the performance of the Buddy vehicle excluding the introduced acquisition noise. The virtual diver experiment was divided into three groups: a) approach experiment, b) rotation experiment, c) tracking experiment.

During the experiment the desired monitoring point is located on the opposite side of circle. The horizontal path taken by the vehicle is shown in Figure 4.6. Observe the similarity of individual approaches independently of the distance. Depending on the approach vector, either a south or a north overtake is taken. Note that the south overtake experiments exhibit undershoots during path following. These might be attributed to influences of the debug optic cable, coming from the north-east, as similar behaviour is not noticed on the north overtake. The distance distribution along the path is shown in Figure 4.6c. In the experiment the vehicle is considered to be on the path after it enters the distance of R ± 2.5%, where R is the safety radius. The maximum distance error is almost ±0.9 m due to undershoots on the southern overtake. However, 50 % of the values are located inside ±0.1 m. The experiment shows that path, rather than point, convergence is preferred. Standard positioning controllers without collision detection, e.g. dynamic position, would converge directly towards the point causing them to pass through the safety radius.

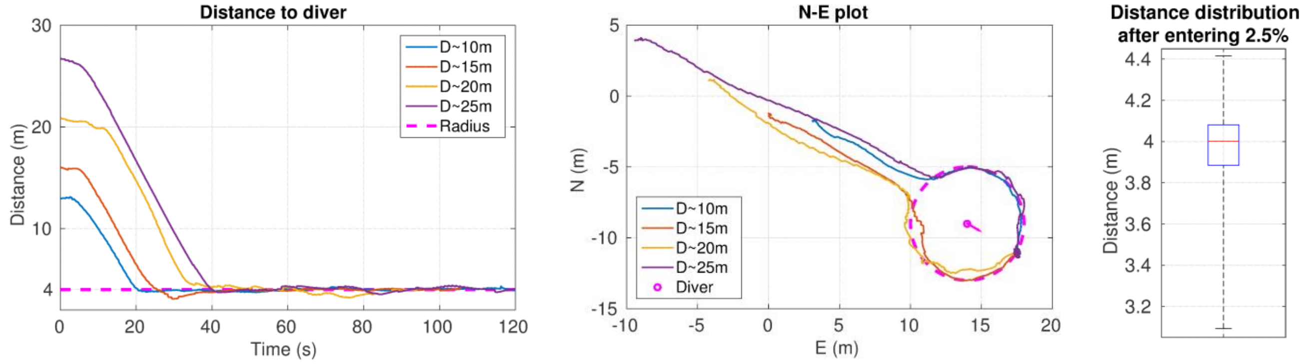


*(a)* *(b)* *(c)*

*Figure 4.6 - Four approach experiments are shown in the sub-figures. (a) shows the distance reduce to the safety radius. The distance distribution along the path is shown in (c) and the vehicle trajectory in (b). The box-plot shows the median value with the box be*

The rotating experiment is shown in Figure 4.7. The normalized path error in Figure 4.7a shows the average for each transition in a full line while individual transitions are plotted with dashed lines to maintain clarity of presentation. The distance to the diver appears to be noisier with increased step-sizes with maximum path error up to 0.4 m. However, 50% of samples are within a much smaller region around the ideal path. Transient time is larger than is required for tight monitoring. On sharp turns the vehicle will fail to monitor the diver frontally for longer times. Gains can be additionally adjusted to achieve a wider period during which the maximum sway speed is used. However, to drastically decrease transient time, different solutions have to be sought.

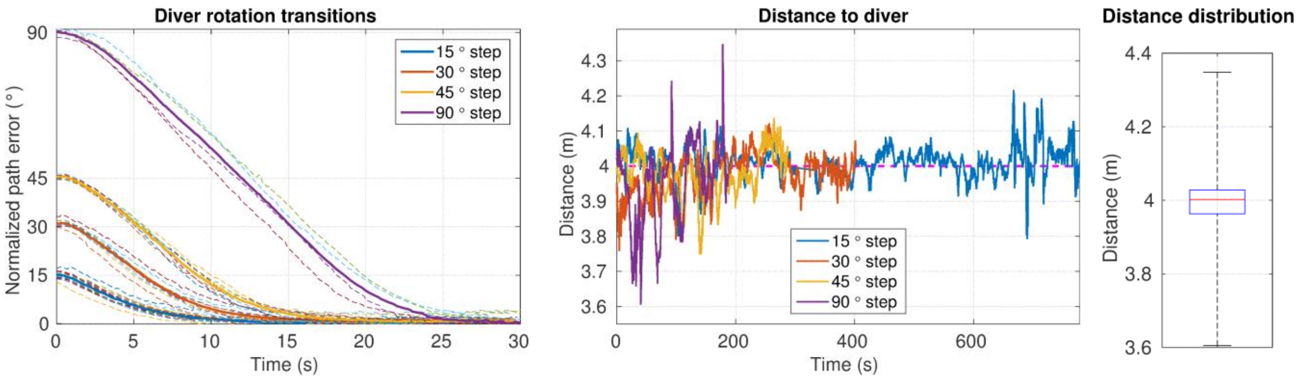


*(a)* *(b)* *(c)*

*Figure 4.7 - Forty-eight experiments are shown in the above figures. The normalized path (angular) error is shown in Figure 4.8*

The results of both tracking tests are shown in Figure 4.9. The virtual diver moved at 0.2 m/s. Observe that the vehicle adapts to changes in the virtual diver orientation during the zigzag part. In the second part the vehicle begins to overtake the diver. Note that 20 m are needed for the vehicle to start getting in front of the diver. This is attributed to the fact that the maximum achievable sway speed is ≈ 0.3 m/s. The problem again indicates the need for alternative design, to maximize sway speed, or a different overtaking strategy. Assuming that maintaining constant focus on the diver is not obligatory the vehicle can be made to favour surge over sway during such manoeuvres as in surge it is three times faster. Maximal distance keeping errors are worse than expected and could partially be contributed to optical cable entanglement, e.g. at 150 s for the first experiment. However, repeatable offset from the desired path is visible after 200 s which coincides with the sharp turn of the virtual diver. During the sharp turn of the diver the vehicle fully reverses the direction of movement. Although the maximum errors are larger, at least 50 % of samples fall into ±0.2 m around the ideal path.

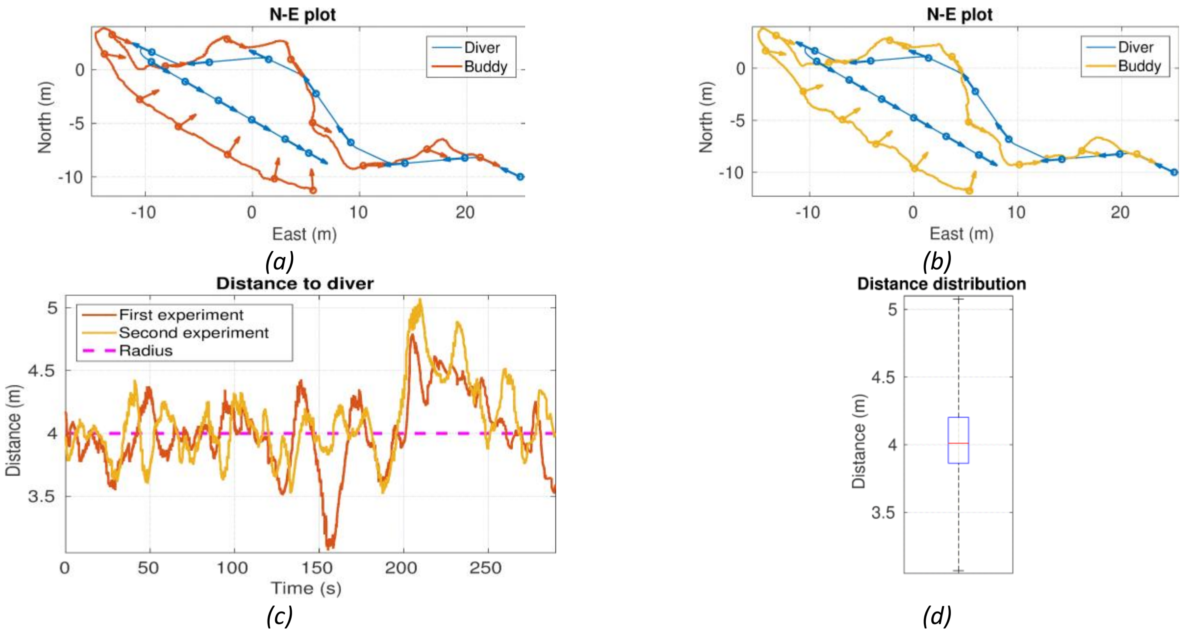


*Figure 4.9 - Two tracking experiments are shown in the figure. The North-East plots for each experiment are shown in (a) and (b). Distance to the diver and its distribution are shown in (c) and (d), respectively.*

The USV diver experiments were carried out only as proof of concept as opposed to the repeatable experiments with the virtual diver. The USV was detected from Buddy using the ARIS sonar and no sonar data filtering was used during the shown experiments. During future experiments the goal will be to include data fusion of sonar, USBL and the diver kinematic model.

Figure 4.10 shows an overtaking example where the USV turns twice by 90 degrees and Buddy is required to overtake the USV in order to position itself in front. The distance distribution shows that the vehicle has a static tracking error. This is due to lack of a data fusion filter which estimates the USV diver speed. Normally, this speed is used as feed-forward to reduce the tracking offset. Around 50% of the time the vehicle is within ±0.3 m around the median tracking distance.

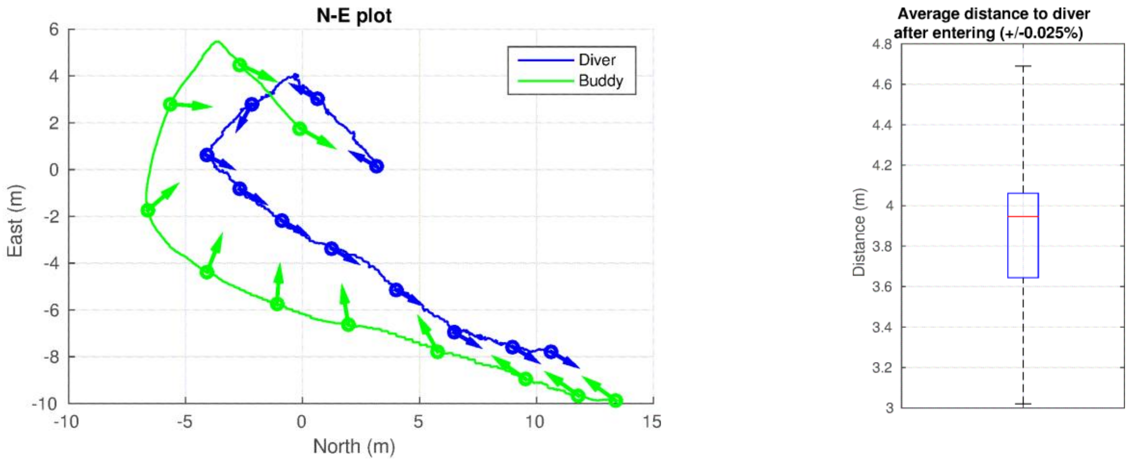


(a) (b)

*Figure 4.10 - Overtaking example from the USV tracking experiment. The North-East is shown in (a) and the distance to diver distribution is shown in (b).*

*Diver guidance* has to be tested on real divers in order to analyze the intuitiveness of guidance by adjusting vehicle relative position. This is incorporated directly into the developed controller via $\mu^*$. Adjusting the position along the safety circle can therefore be calculated based on the relative position of the target, diver and buddy. An aiding method or fallback is guidance by use of indicators on the Buddy tablet which is easily visible to the diver.

# 5 Conclusions

This deliverable has described the design and implementation of the Buddy guide functionality that provides the CADDY system the capability of guiding the human divers to a goal, further testing will be done in October 2016, with the whole system working, aiding a human diver.

# 6 Literature

Abreu, Pedro Caldeira, and António Manuel Pascoal. 2015. "Formation Control in the scope of the MORPH project. Part I: Theoretical Foundations." *Proc. 4th IFAC Workshop on Navigation, Guidance and Control of Underwater Vehicles.* Girona, Spain.

Fahimi, F., H. Ashrafiuon, and C. Nataraj. 2003. "Obstacle Avoidance for Spatial Hyper - Redundant Manipulators Using Harmonic Potential Functions and the Mode Shape Technique." *Journal of Robotic Systems, Wiley Subscription Services, Inc., A Wiley Company* 23-33.

Khatib, O. 1985. "Real-time obstacle avoidance for manipulators and mobile robots." *Robotics and Automation. Proceedings. 1985 IEEE International Conference on.* 500-505.

Kim, J. O., and P. K. Khosla. 1992. "Real-time obstacle avoidance using harmonic potential functions." *IEEE Transactions on Robotics and Automation* 338-349.

Kuethe, A. M., and C. Chow. 1985. *Foundations of Aerodynamics: Bases of Aerodynamic Design.* Wley.

Latombe, Jean-Claude. 1991. *Robot Motion Planning.* Kluwer Academic Publishers.

Miskovic, N., D. Nad, N. Stilinovic, and Z. Vukic. 2013. "Guidance and control of an overactuated autonomous surface platform for diver tracking." *Control & Automation (MED), 2013 21st Mediterranean Conference on.* 1280-1285.

Nađ, Đula, Nikola Miskovic, Henrique Silva, Miguel Ribeiro, Jorge Ribeiro, Pedro Abreu, and António Pascoal. 2016. "Cooperative Surface/Underwater Navigation for AUV Path following mission." *10th IFAC Conference on Control Applications in Marine Systems (CAMS).* Trondheim, Norway: IFAC.